Journal of The Electrochemical Society, **153** (1) C37-C50 (2006)
0013-4651/2005/153(1)/C37/14/$15.00 © The Electrochemical Society, Inc.

Electrodeposition of Cu on Ru Barrier Layers for Damascene Processing

T. P. Moffat,[a,*,z] M. Walker,[b] P. J. Chen,[a] J. E. Bonevich,[a] W. F. Egelhoff,[a] L. Richter,[b] C. Witt,[c] T. Aaltonen,[d] M. Ritala,[d] M. Leskelä,[d] and D. Josell[a]

[a]*Materials Science and Engineering Laboratory, and* [b]*Chemical Science and Technology Laboratory, National Institute of Standards and Technology, Gaithersburg, Maryland 20899, USA*
[c]*Enthone Division, Cookson Electronics, Orange, Connecticut 06516, USA*
[d]*Laboratory of Inorganic Chemistry, University of Helsinki, Helsinki, Finland*

Superfilling of submicrometer trenches by direct copper electrodeposition onto physical vapor deposited and atomic layer deposited Ru barriers is demonstrated. The Cu nucleation and growth mode is found to be sensitive to the oxidation state of the Ru surface as well as the copper deposition parameters. Depending on the processing conditions, Cu deposition may or may not occur competitively with oxide reduction. Failure to remove the air-formed 3D oxide film results in Volmer-Weber (island) growth and consequently poor trench filling, as well as poor adhesion between Cu and Ru. In the case of thin resistive oxide-covered Ru seed layers, the "terminal effect" further exacerbates the difficulties in obtaining a compact, fully coalesced Cu film because the rate of Ru oxide reduction is decreased along with the density of Cu nuclei. In contrast, Cu deposition on a reduced "oxide-free" Ru surface results in more rapid coalescence involving the formation of a wetting Cu underpotential deposition layer. Electrochemical reduction of the oxidized Ru seed layer in a deaerated sulfuric acid solution, followed by rapid wet transfer to a Cu plating bath, enables robust superfilling of trenches and improved adhesion between Cu and Ru. Early film coalescence is favored by deposition at high ($\eta \approx -0.25$ V) overpotentials.
 [DOI: 10.1149/1.2131826]

Manuscript submitted June 3, 2005; revised manuscript received September 9, 2005. Available electronically December 2, 2005.

As the width of on-chip interconnect wiring shrinks below the 70 nm length scale, attention is being focused on strategies that minimize increases in the resistance of the conductors. Current interconnects include an outer diffusion barrier such as Ta and a physical- or chemical vapor deposited (PVD or CVD) Cu seed layer in addition to the electrodeposited Cu conductor. The diffusion barrier prevents property-degrading migration of the Cu conductor into the surrounding dielectric. The Cu seed layer is required due to poor nucleation of electrodeposited Cu on conventional oxidized Ta barriers.[1,2]

In the early years of Cu damascene technology, failures related to seed layer processing and corrosion were responsible for many integration difficulties. Decreasing feature size and increasing aspect ratios are leading to new challenges in obtaining with uniformity of coverage. Dimensional shrinkage means that barrier materials are also occupying an increasing fraction of the cross-sectional area of the conductors. This is highly undesirable because the intrinsic electrical and thermal conductivity of Ta is almost an order of magnitude smaller than that of Cu. Ru and other Pt-group elements have been suggested as possible replacement candidates.[3-5] Ru is particularly promising because bulk phase Ru and Cu are immiscible and the thermal and electrical conductivities of Ru are twice those of Ta.

The ability to directly deposit smooth compact Cu films on Ru gives rise to the possibility of a seedless superfilling process. Our preliminary work in this area revealed an interesting sensitivity of submicrometer feature filling behavior to the manner in which the Ru barrier layer was treated prior to plating. Three limiting condition are summarized in the cross-section field-emission scanning electron microscope (FE-SEM) images shown in Fig. 1. The first case (A) exemplifies the desired result, namely, early coalescence of the electrodeposited Cu film followed by bottom-up superfilling that is indistinguishable from growth on a conventional Cu seed layer. The second case (B) corresponds to Volmer-Weber (island) growth characteristic of poor Cu wetting of Ru with consequently poor trench filling. An intriguing, but most likely spurious, third case (C) is selective growth within the features; while negligible deposition occurs on the free surface, this filling behavior was only encountered in 2 of more than 200 specimens. These observations demonstrate sensitivity to processing details that must be clarified in order to establish a robust manufacturing process. To date, there are two publications that deal with the effect of potential[3] and current density,[6] respectively, on the morphology of Cu deposited on Ru in terms of Volmer-Weber growth. However, a survey of the electrochemical and vacuum literature indicates that Cu effectively wets Ru surfaces[7-10] and a variety of strained overlayer structures[11-13] exists, at least on Ru(0001), all of which suggests that a Stranski-Krastanov growth mode (initial layer-by-layer followed by 3D growth) might be operative. Of course, transferring a Ru-seeded wafer through the laboratory ambient results in its oxidation and the impact on subsequent Cu deposition must be accounted for.

Ru oxidation is a sensitive function of its microstructure, with pronounced differences in behavior noted between Ru(0001), bulk and thin-film polycrystalline Ru, as well as electrodeposited Ru surfaces.[7,14-19] In fact, reports of the charge associated with electrochemical oxidation of Ru and its reduction vary by more than an order of magnitude. Such variation may be attributed to a combination of effects ranging from inherent crystalline anisotropy of the oxidation reaction, to preferential oxidation associated with surface defects[14-16] and/or large variation in the surface area associated with the respective as-deposited thin film structures.[7,14-19] In the case of PVD films, the refractory nature of Ru (T_{melt} = 2773 K) provides limited surface mobility during vapor deposition at room temperature that can lead to significant density variations within the film as well as surface roughness. The effect is accentuated on sloping surfaces such as via and trench sidewalls, where the resulting film takes on the porous film characteristics associated with glancing angle deposition.[20] Thus, significant variation in film structure and corresponding properties can be anticipated under such circumstances. Atomic layer deposition (ALD) and related CVD methods offer the prospect of more uniform barrier layers than provided by PVD.

The chemistry and microstructure of the oxide formed on Ru is known to be a sensitive function of the oxidation conditions.[8,14-16,21] The resulting microstructures can vary from well-ordered oxide to fine grained with variable hydroxide content depending on the details of thermal or electrochemical oxidation. Interfacial water, and thus relative humidity, appears to play a significant role in room temperature atmospheric oxidation.[22,23] Indeed, variations in the humidity and exposure time between various specimens may account for much of the dispersion in filling experiments (e.g., Fig. 1).

In this paper, the effect of different pretreatments and electrodeposition conditions on the nucleation and growth of Cu on Ru

* Electrochemical Sociey Active Member.
z E-mail: thomas.moffat@nist.gov

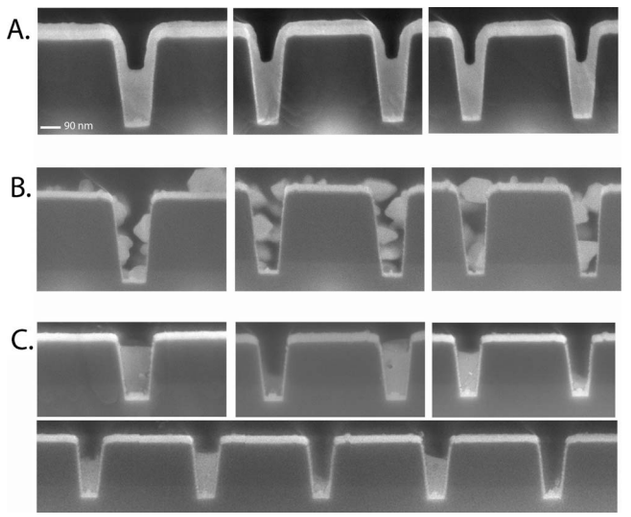

Figure 1. Morphological evolution during Cu electrodeposition on a Ru barrier layer is a significant function of the chemical state of the Ru as evidenced by cross-section FE-SEM images of trench filling (three different aspect ratios shown). Cu was deposited at −0.2 V from a PEG-Cl-SPS electrolyte. (A) Deposition on freshly evaporated Ru results in early coalescence of the Cu overlayer and robust feature superfilling (t = 7.6 s). (B) In contrast, more extensive oxidation and contamination of the Ru layer results in poor wetting of the Cu during deposition (t = 10 s). (C) Infrequently, spatially distributed contamination of the barrier layer results in selective nucleation and growth from the trench bottom (t = 8.3 s). The stochastic nature of this intriguing nucleation process is evident.

will be examined using a combination of electroanalytical, spectroscopic, surface imaging, and feature filling experiments.

Experimental

Cu deposition was characterized on Ru thin films produced by both electron-beam evaporation (PVD) and atomic layer deposition (ALD). For electroanalytical and spectroscopic (X-ray photoelectron spectroscopy, XPS, and ellipsometry) studies, planar PVD films of three different thicknesses were examined. The PVD films were grown at room temperature at a rate of 0.1 nm/s in a mid 10^{-6} Pa (10^{-8} Torr) vacuum. A thin Ti layer was used to enhance adhesion between the native oxide of the Si(100) substrate and the Ru barrier layer. The dimensions of the respective films were 100 nm Ru/5 nm Ti, 27 nm Ru/1 nm Ti, and 6.5 nm Ru/2 nm Ti. The as-deposited planar films were stored in a conventional wafer carrier for periods ranging from a few minutes to several weeks. The films were examined in cross section by transmission electron microscopy (TEM) and in plan view by FE-SEM. As shown in Fig. 2, the limited surface mobility of refractory metals at room temperature results in the development of significant surface roughness that scales with film thickness. The grain size of the thin 6.5 nm Ru film is on the order of the film thickness, while the 100 nm film exhibits columnar growth with an upper bound on the grain size of 20 nm. The thicker film is substantially rougher and exhibits cracking attributable to growth-related stresses.

A variety of electroanalytical experiments was performed with the PVD Ru films. Electrodes were fabricated from diced Ru/Ti/SiO_x-Si(100) squares supported on a Cu plate with a Cu foil making a symmetric radial electrical contact to the Ru film. The construct was masked with 3M plater's tape, leaving an exposed Ru circular area of 2.91 cm^2. Experiments were performed using either a saturated mercury/mercurous chloride (SCE) or saturated mercury-mercurous sulfate (SSE) reference electrode. All reported experimental values are referred to the SCE scale. The oxidation and reduction of Ru was studied in an electrolyte comprised of 1.8 mol/L H_2SO_4 + 1 mmol/L NaCl that corresponds to the acid matrix used

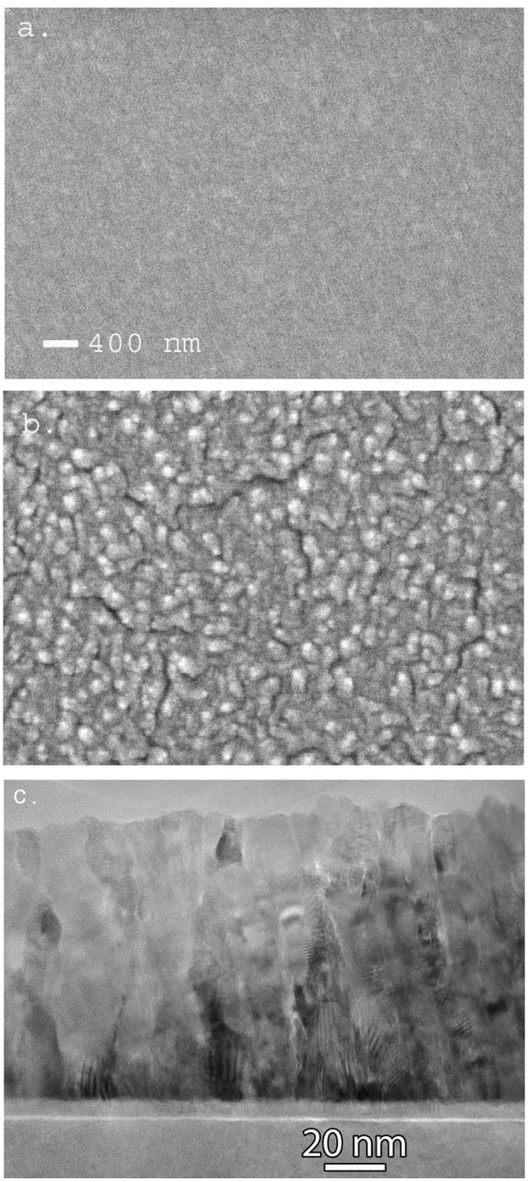

Figure 2. FE-SEM of the surface of (a) 6.5 nm and (b) 100 nm thick evaporated Ru film. (c) TEM cross section image of the 100 nm thick Ru film.

for Cu superfilling. Underpotential deposition (upd) of Cu on Ru has been previously reported[7-10] and the impact of various surface treatments on Cu upd were examined following the addition of 1–10 mmol/L $CuSO_4$ to the matrix. The upd reaction was also used to quantify the electroactive area of the PVD films.

XPS was utilized to examine adsorption of various plating additives, Cl, PEG, and SPS, on the reduced and oxidized Ru surface, respectively. Emersed samples were first rinsed with water and then dried with a tetrafluoroethane duster before transferring to UHV-XPS chamber. Corresponding in situ ellipsometric experiments were performed and are reported in a companion manuscript.[24] These methods were also used to probe Cu upd on the respective surfaces.

A key aspect of this work involves examination of the effect of surface preparation on Cu deposition under superfilling conditions. Experiments on planar electrodes were performed in 1.8 mol/L H_2SO_4 + 0.24 mol/L $CuSO_4$ + 1 mmol/L NaCl + 88 μmol/L PEG (polyethylene glycol, 3400 Mw) with/without 50 μmol/L SPS (Bis-(3-sulfopropyl)-disulfide, disodium salt, $Na_2[SO_3(CH_2)_3S]_2$, Ra-

schig). The full additive combination PEG-Cl-SPS was used for feature filling experiments. Experiments were also performed using SPS or MPS [$NaSO_3(CH_2)_3SH$, Aldrich[e]] derivatized electrodes. Over 200 PVD and ALD Ru-seeded patterned trench specimens were examined after Cu deposition. Lithographically patterned SiO_x/Si wafers were provided by International Sematech. A tilting sample stage was used to enable effective trench sidewall coverage of Ru during the PVD process as detailed previously.[25] Representative specimens had 27 nm of Ru on the free surface, and 3 to 4 nm on the sidewalls. With a few exceptions, Cu was electrodeposited on the Ru-seeded patterned specimens within the first hour of exposure to the laboratory ambient. A more limited set of filling experiments was performed on specimens with an ALD Ru barrier layer. The ALD films were grown at 350°C using $RuCp_2$ and oxygen as the precursors.[26] A thin Al_2O_3 layer was used to enhance nucleation and adhesion of the Ru film. The thickness of the ALD Ru films was 18 to 23 nm and the thickness of the Al_2O_3 film was about 4 nm. Cross sections of trench filling were studied by FE-SEM, as were the morphologies of Cu deposits grown on planar substrates. A simple peel test was used to qualitatively examine the effect of various surface pretreatments on Cu/Ru adhesion.

The large resistance of the thin Ru seed layers, 27 and 6.5 nm, gives rise to a substantial iR drop during electrodeposition. The so-called "terminal effect" influences deposit morphology through its potential-dependent nature convoluted with the surface conditions. The combination of electroanalytical experiments, deposit morphology, and Cu/Ru adhesion tests enables the effect of surface pretreatments and finite seed-layer resistivity to be evaluated.

Results and Discussion

Oxide formation on Ru and its reduction.— As-received PVD Ru is covered with an air-formed oxide film. Immersion into 1.8 mol/L H_2SO_4 + 1 mmol/L NaCl that is open to the laboratory ambient yields an open-circuit potential ranging from 0.69 to 0.76 V SCE that reflects coupling between the oxidizing power of dissolved oxygen and the oxide film. Subsequent deaeration with N_2 or initial immersion in N_2-saturated solution yields a similar result, indicating the air-formed oxide film is potential determining. The surface film can be removed by polarization at negative potentials, typically in or approaching the hydrogen evolution region. An effective activation treatment involves stepping the potential to −0.2 V SCE for 30 s. The activation process was characterized voltammetrically as shown in Fig. 3. For a 100 nm thick Ru film the reduction process is evident as the reduction wave near −0.240 V, SCE, while for the 6.5 nm thick film the peak potential is centered at −0.150 V SCE. Integration of the negative-going voltammetric cycle yields a charge of 30 mC/cm^2 for the 100 nm Ru film, while ≈3 mC/cm^2 is observed for the 6.5 nm Ru film. The tenfold difference in charge may be at least partly attributed to the significantly greater roughness of the 100 nm specimen (i.e., Fig. 2). The origin of the shift in the peak potential remains unresolved but may be related to difference in post-UHV deposition aging time. Performing the same voltammetric experiment in a N_2 deaerated electrolyte yields the same general result (minus a small dc offset associated with the exclusion of diffusion limited O_2 reduction), leaving H^+/H_2, capacitive charging, hydrogen insertion, and/or reduction of a surface film as the only operable processes. A companion ellipsometry study reveals a clear optical signature of the oxide removal process.[24]

Once an as-received Ru electrode is activated in the hydrogen evolution region (e.g., −0.2 V SCE for 30 s), the extent of subsequent oxidation at more positive potentials can be easily examined by voltammetric sampling. In a typical experiment the electrode is held at fixed potential for 120 s, voltammetrically probed, and then

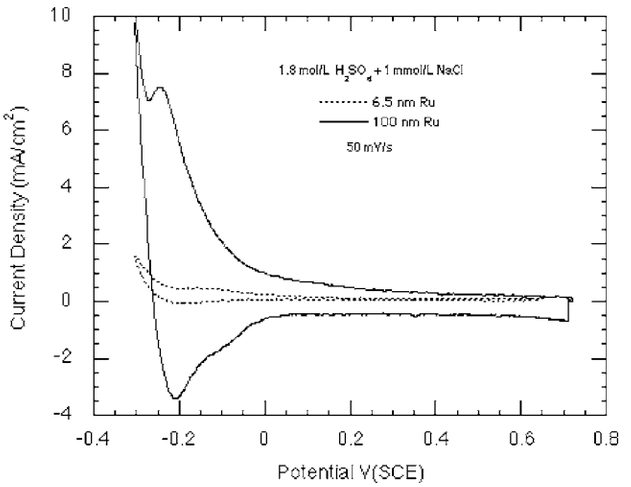

Figure 3. Voltammetry revealing the reduction of the air-formed oxide on evaporated Ru films exposed to air for more than one week. The difference in the magnitude of the reduction wave chiefly reflects differences in the surface area due to roughness.

the process is repeated after progressively stepping to higher potentials. For oxidation below 0.5 V SCE a broad reduction peak centered near 0.17 to 0.18 V SCE is apparent as shown in Fig. 4. Integration yields an upper bound for the total reduction charge for the negative-going sweep of 5.5 mC/cm^2 for the 100 nm Ru film, while 0.9 mC/cm^2 is measured for the 6.5 nm Ru film. Extended polarization at 0.5 V leads to only a slight increase in the peak intensity of the reduction wave. Integrating between 0.5 and −0.150 V SCE yields a more precise evaluation of the reduction wave charge, giving a value of ≈4 mC/cm^2 for the 100 nm Ru and ≈0.45 mC/cm^2 for the 6.5 nm film. Prior work with polished polycrystalline, as well as single-crystal Ru electrodes, indicates that oxidation in this potential regime is a one-electron process

$$Ru + H_2O \rightarrow RuOH + H^+ + e^-$$

more or less chemically reversible, and constrained to the monolayer level ≈0.26 mC/cm^2.[7,14,15] The apparent charge discrepancy may be attributed to a combination of increased surface area and defect density of the PVD films.[7,17-19] Using the charge of monolayer oxi-

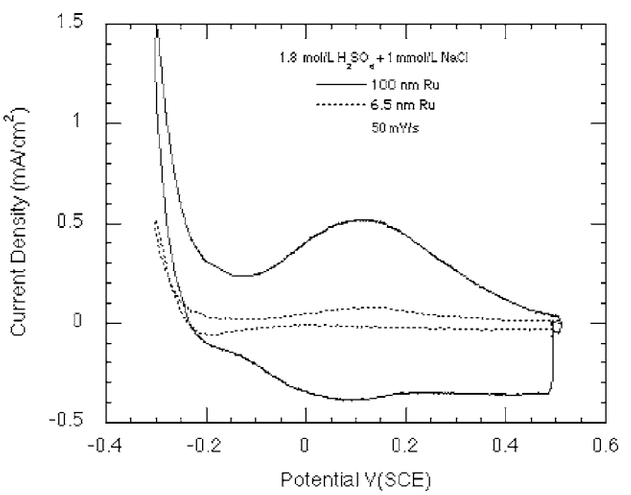

Figure 4. Voltammetry of Ru after activation at −0.2 V for 30 s. The monolayer oxide reduction peak centered at 0.1 V may be used to quantify the relative electroactive area of the two electrodes.

[e]Product names are included only for accuracy of experimental description. They do not imply NIST endorsement.

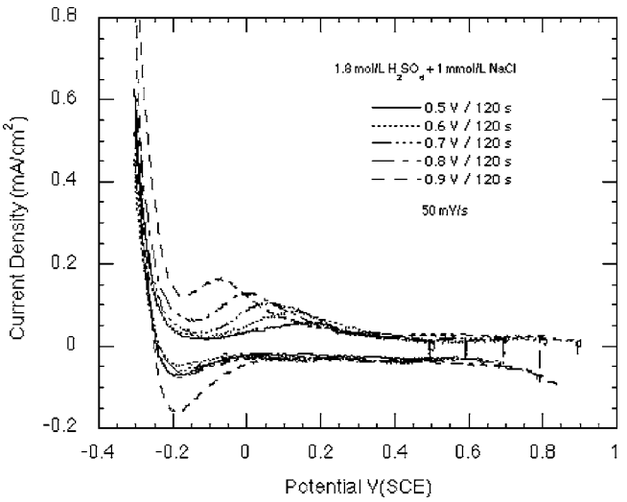

Figure 5. Oxidation of Ru at higher potentials results in an increase in oxide thickness and its resistance to subsequent reduction as reflected by the increase in magnitude and displacement of the reduction wave toward more negative potentials.

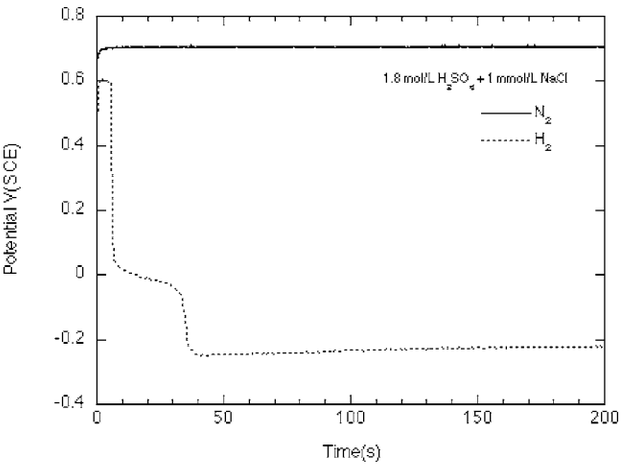

Figure 6. The air-formed oxide on Ru yields an open-circuit potential near 0.7 V. Electrode activation may be easily obtained by immersion in H_2-deaerated electrolyte where the potential is pinned at the reversible H^+/H_2 potential.

dation for area calibration or scaling indicates that the electroactive area of 100 nm thick Ru is 15 times greater than its geometric projection, while the roughness factor of the 6.5 nm film is 1.7. Similar roughness effects have been previously noted in studies of electrodeposited Ru films.[7,17-19] Likewise, coarsening effects have also been reported, suggesting some degree of surface rearrangement accompanies repetitive oxidation and reduction.[7,17-19] Oxidizing the electrode at progressively higher potentials results in expansion of the reduction wave and its displacement toward more negative potentials as shown in Fig. 5. The reduction wave charge increases monotonically with oxidation potential, doubling in value between 0.5 and 0.9 V SCE. Following oxidation at a given potential for 120 s, the position and shape of the corresponding reduction wave is only a slight function of any additional oxidation time that is limited to hundreds of seconds. The evolution of the peak position and shape of the reduction wave for the electrochemically oxidized specimens is indistinguishable between the two Ru films. For the 6.5 nm thick Ru sample, electrochemical oxidation near 0.9 V SCE yields a reduction wave that is similar in shape and position to that observed for the aged as-received air-formed film, although the associated charge is reduced by a factor of 3.

Spontaneous activation in the H_2*-deaerated electrolyte*.— An alternative to potentiostatic electrode activation involves immersion of the electrode into a solution deaerated with H_2 whereby the steady-state potential is set by the proton/hydrogen reaction. This is shown in Fig. 6, where the potential of an immersed air-oxidized Ru electrode moves from 0.69 to −0.24 V SCE. The brief arrest or plateau near 0 V SCE is ascribed to oxide reduction and thus activation of the Ru electrode. In the presence of Cu^{2+} an additional mixed potential can be established that should be capable of seeding Ru with Cu. From another perspective, judicious choice of an alternative reducing agent might permit a process that combines oxide reduction with continuous electroless Cu plating.

Cu upd.— Insight into the electroactive area and state of thin film Ru electrodes may be obtained by studying surface limited underpotential deposition (upd) reactions. Previously, this strategy has been widely used to characterize electrocatalyst, e.g., H^+/H upd on Pt. In the present case, Cu upd on Ru provides a natural avenue for exploring the effect of various electrode pretreatments on the wetting behavior and subsequent growth of bulk Cu. For these studies a Ru electrode was first activated at −0.2 V for 30 s in 1.8 mol/L H_2SO_4 + 1 mmol/L NaCl. The potential was then stepped to 0.5 V SCE, where monolayer oxide formation occurs, and then 9 mmol/L $CuSO_4$ was added to the electrolyte to study the Cu deposition process. Cu upd on the activated 6.5 nm thick Ru manifests as the reduction wave centered at 0.06 V SCE in Fig. 7a. The upd process on activated Ru is kinetically hindered as evident from the 0.065 V separation between the deposition and stripping wave in Fig. 7b. Reduction of the monolayer oxide species also occurs in this regime as revealed by the background voltammogram (Fig. 7a and Fig. 4). Indeed, it is possible that the oxide desorption process controls the onset of the Cu upd reaction. Integration of the upd wave between 0.5 and 0 V SCE, followed by subtraction of the background current associated with monolayer oxide reduction, yields a charge of 1 mC/cm^2. Prior work[7] using mechanically polished in H_2SO_4/Cl reports a charge of ≈0.6 mC/cm^2 ascribed to a close-packed monolayer of Cu(111)/Ru(0001). Other experiments in perchloric acid also yield 0.6 mC/cm^2.[9,10] The similar work functions of Cu and Ru in combination with voltammetric,[15,21] and radiotracer[27] studies suggest that Cl adsorption is anticipated in the current system and that variations in anion coverage between Ru versus Cu will exert a secondary influence on the total charge exchanged during Cu upd on Ru. Further work will be required to verify this view. Taking 0.6 mC/cm^2 as representative of a monolayer Cu upd charge yields a roughness factor of 1.7 for the 6.5 nm Ru film, in agreement with the value derived previously from oxide reduction. The onset of bulk Cu deposition occurs below 0 V SCE and is diffusion limited beyond −0.175 V SCE. The upd layer formed at 0.05 V SCE for 60 s was examined by XPS. Specimen transfer from the electrochemical cell to UHV involved exposure to air, water rinsing, and drying with tetrafluoroethane duster. The Cu(2p) peaks of the monolayer film are evident in Fig. 7c. Comparison of the ratio of the integrated intensity of the Cu($2p_{3/2}$) and Ru($2d_{5/2}$) is congruent with formation of a Cu upd layer or rather its oxidized variant, e.g., Cu_2O, on the emmersed surface.

Intentional oxidation of Ru, at 0.9 V SCE for 120 s, greatly inhibits the subsequent Cu upd process; note the missing redox waves in Fig. 7b. The same conclusion is reached for air-oxidized Ru, where XPS analysis (Fig. 7c) of a specimen emersed after 60 s at 0.1 V reveals only a trace level of Cu on the surface. Thus, significant Cu upd does not occur on the 3D oxide that spontaneously forms on exposure of Ru to humid air or by electrochemical oxidation between 0.6 and 0.9 V SCE. This result is in agreement with previous work where Cu upd is readily observed on mechanically polished Ru but suppressed on electrochemically oxidized Ru,[7] and completely absent of RuO_2.[28] In contrast, there is a recent report

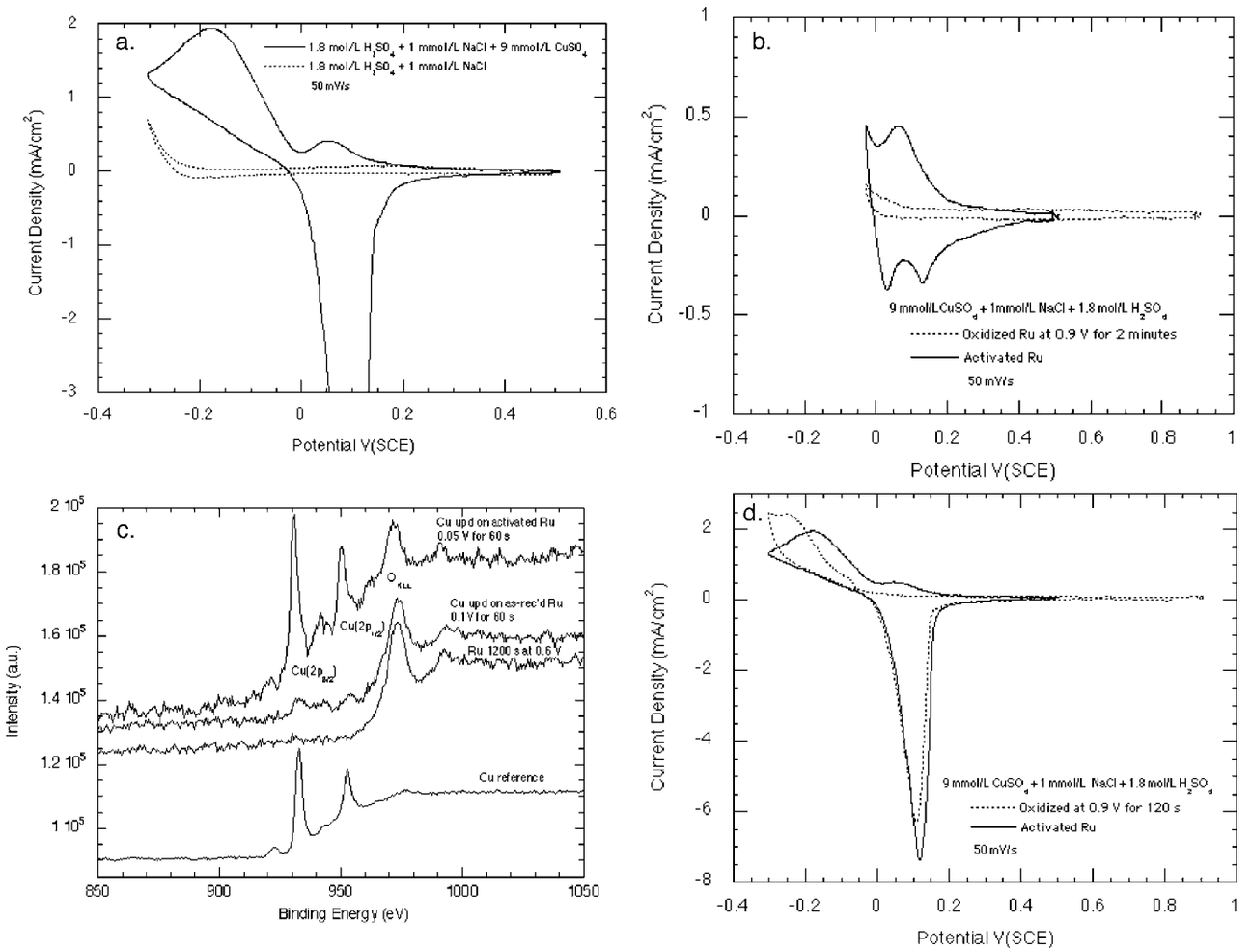

Figure 7. (a) Voltammety of an activated Ru (6.5 nm) electrode showing Cu upd at ~0.06 V followed by bulk Cu deposition and its subsequent stripping. (b) Oxidation of Ru at 0.9 V blocks the Cu upd reaction. (c) XPS (2p) spectrum of the emmersed Cu upd layer on activated Ru versus its absence on air oxidized as-received Ru. (d) Bulk Cu deposition occurs on the oxidized surface at more negative potentials.

suggesting that Cu upd may occur on colored hydrous RuO_xH_y films grown at 1.35 V SCE, although much remains to be understood.[29]

While impeding Cu upd, the thin oxide film grown at 0.9 V SCE does not prevent bulk Cu deposition. As shown in Fig. 7d, the nucleation and growth of bulk Cu on oxidized Ru occurs readily at potentials below 0.0 V. Importantly, this also corresponds to the potential regime where oxide reduction occurs (Fig. 3 and Fig. 5). Thus, it is unclear whether Cu nuclei are forming on top of the oxide or at sites of oxide reduction. As shown in Fig. 7d, the diffusion-limited peak current density slightly exceeds that for an activated electrode. It most likely reflects a difference in the nucleation and thereby morphology of bulk Cu deposited on activated Ru versus oxide-covered Ru. Prior work has shown RuO_2 to be an effective catalyst for hydrogen production, even in the presence of Cu that otherwise is known to strongly poison conventional Pt electrocatalyst.[28] This result implies that Cu deposition on RuO_2 grows as a rough noncoalescent overlayer that does not substantially block electrolyte access to the substrate surface. In this study a similar result is reported for Cu deposition on oxidized Ru.

The Cu upd process presents numerous possibilities for surface modification of Ru with additives relevant to superfilling applications. From a surface analytical perspective, interactions between Cu upd and plating additives can be studied free of the measurement challenges associated with study of the moving interface associated with bulk Cu deposition or dissolution. A prime example is the impact of PEG additions on Cu upd. Ellipsometry was used to study PEG-Cl adsorption on the activated Ru surface. In agreement with expectations based on pzc (point of zero charge) arguments,[30] PEG-Cl coadsorption occurs on activated Ru held at 0.05 V SCE.[24] Likewise, PEG-Cl coadsorption occurs on top of the Cu upd layer regardless of the order of addition of the respective components, PEG/Cu^{2+}, to the electrolyte.[24] However, at higher potentials $\approx$0.5 V SCE the PEG layer is disrupted by the formation of an oxide monolayer.[24] As shown in Fig. 8a, PEG coadsorption does not affect the upd peak potential, although a reduction in the peak current is observed. In contrast, the peak current of the desorption wave is only slightly attenuated by PEG coadsorption, while a 50 mV shift of the peak potential to more positive potentials indicates a degree of stabilization of the upd Cu/Cl is provided by coadsorbed PEG. As suggested earlier, the absence of any shift in the peak potential of the deposition wave is consistent with the kinetics of the Cu upd being controlled by monolayer oxide reduction, as indicated by the background voltammogram shown in Fig. 8a.

Importantly, when the potential is swept to more negative values, the coadsorbed PEG-Cl–Cu upd layer provides significant inhibition of Cu overpotential deposition as indicated in Fig. 8b. A sketch of this process is given in Fig. 9, where PEG-Cl-Cu upd forms a wetting layer on the activated Ru surface. This layer inhibits the subsequent deposition of bulk Cu in a manner analogous to growth suppression on a bulk Cu electrode.

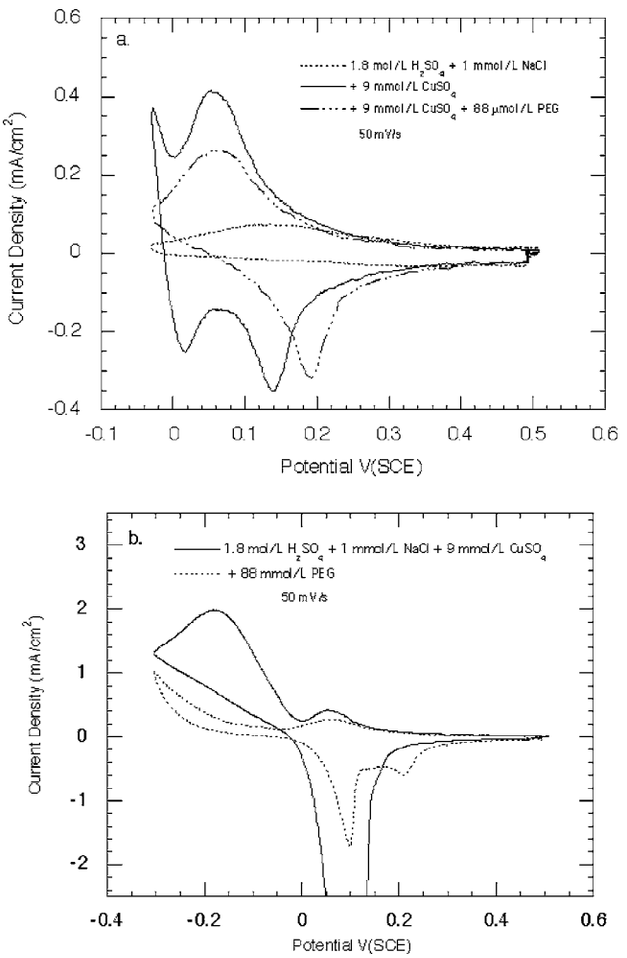

Figure 8. (a) Voltammetry showing the effect of PEG on Cu(upd) on Ru. The deposition charge is reduced and the stripping wave is displaced to higher potentials, indicating that PEG coadsorbs during Cu upd. (b) Sweeping to more negative potential reveals the inhibition of bulk Cu deposition provided by PEG addition.

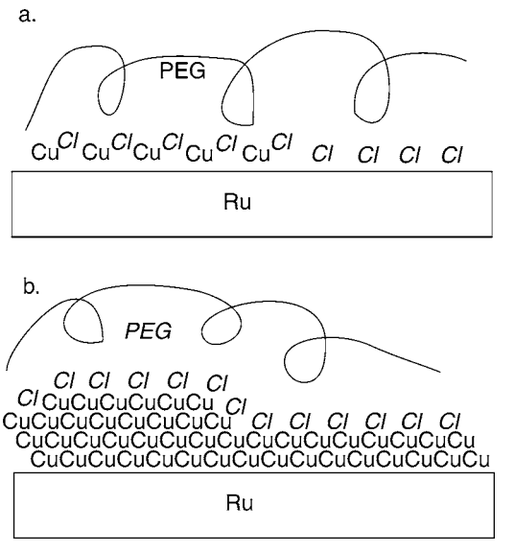

Figure 9. A schematic drawing indicating PEG coadsorption on oxide-free Ru is mediated by adsorbed chloride. Similar observation applies to PEG adsorption on Cu upd/Ru. (b) The Cu upd layer acts a wetting layer for subsequent bulk Cu deposition via Stranski-Krastanov mode.

In contrast, if the activated Ru surface is oxidized at 0.9 V, no upd is evident on the negative-going sweep in the presence of PEG, although the onset of overpotential Cu deposition, shown in Fig. 10a, occurs in a manner analogous to that observed in an additive-free solution. Comparison with the voltammetry in the absence of Cu^{2+} (Fig. 10b) demonstrates that the onset of reduction of the 3D oxide also occurs in the same regime. For some conditions the distribution of nuclei may be correlated with sites of oxide reduction, although this aspect requires further study. In any case, once Cu nuclei do form, PEG-derived inhibition sets in as the potential moves below −0.1 V SCE. The voltammetric response indicates that in the presence of PEG and the 3D Ru oxide, the oxide dominates the early stages of Cu plating behavior, i.e., no Cu upd occurs on the oxidized Ru surface and Cu overpotential deposition is not inhibited. Rather, Cu deposition proceeds by a 3D Volmer-Weber nucleation and growth process as shown schematically in Fig. 11. Subsequently, PEG accumulation and inhibition of further Cu deposition occurs in competition with the dilution of the PEG coverage arising from the rapidly expanding interfacial area of the growing Cu nuclei. The differential area expansion per unit of growth decreases with nuclei size, and eventually PEG completely covers the surface. Depending on the system parameters, this may coincide with nuclei coalescence where the voltammetric response merges with that for an activated Ru electrode, the latter being quite similar to that for a bulk Cu electrode.

Bulk Cu deposition on as-received PVD Ru.— The surface oxide on Ru also affects morphological evolution during Cu deposition from PEG-Cl electrolytes containing the higher Cu^{2+} concentrations that are relevant to damascene feature filling. Slow scan rate voltammetry for Cu deposition on mechanically polished Cu and as-received PVD 100 nm thick Ru substrates is shown in Fig. 12. Both substrates were initially held at 0.08 V SCE for less than 10 s, followed by scanning the potential between 0.1 and −0.45 V SCE. The deposition rate-inhibiting PEG-Cl film forms immediately upon immersion of the Cu electrodes, resulting in a decrease in the Cu deposition rate of two orders of magnitude relative to that in the PEG-free environment.[31,32] In contrast, initial Cu deposition on as-received Ru is not significantly blocked, as evident by the sharp onset of metal deposition at 0.02 V SCE, corresponding to a nucleation overpotential of 0.025 ± 0.005 V. The deposition rate increases with overpotential, with significant PEG-Cl induced inhibition only becoming manifest as the decrease in current between −0.04 and −0.12 V SCE. The subsequent evolution of the current ultimately yields voltammetry coincident with a PEG-Cl inhibited Cu electrode. Increasing the PEG concentration an order of magnitude exerts a negligible effect on the peak current and/or shape, indicating that PEG diffusion to the interface is not rate limiting under these conditions. The total charge associated with the current peak is 0.35 C/cm^2, corresponding nominally to a 128 nm thick Cu layer (if uniformly distributed and there is 100% current efficiency for the Cu^{2+}/Cu deposition reaction). For a given sweep rate, the nucleation potential is practically invariant to changes in the immersion potential between +0.6 and +0.1 V SCE although a slight decrease (<10%) in the integrated charge was noted.

Chronoamperometry was used to further investigate Cu nucleation on as-received Ru. As shown in Fig. 13a, stepping the potential to −0.025 V SCE results in a steady-state current of 0.25 mA/cm^2 for deposition of Cu on Cu similar to that observed voltammetrically. In contrast, on as-received Ru the current jumps to ≈7 mA/cm^2, followed by a gradual decay that merges with the Cu current transient at 800 s. The corresponding charge is 0.770 C/cm^2, twice that associated with the corresponding voltammetric wave.

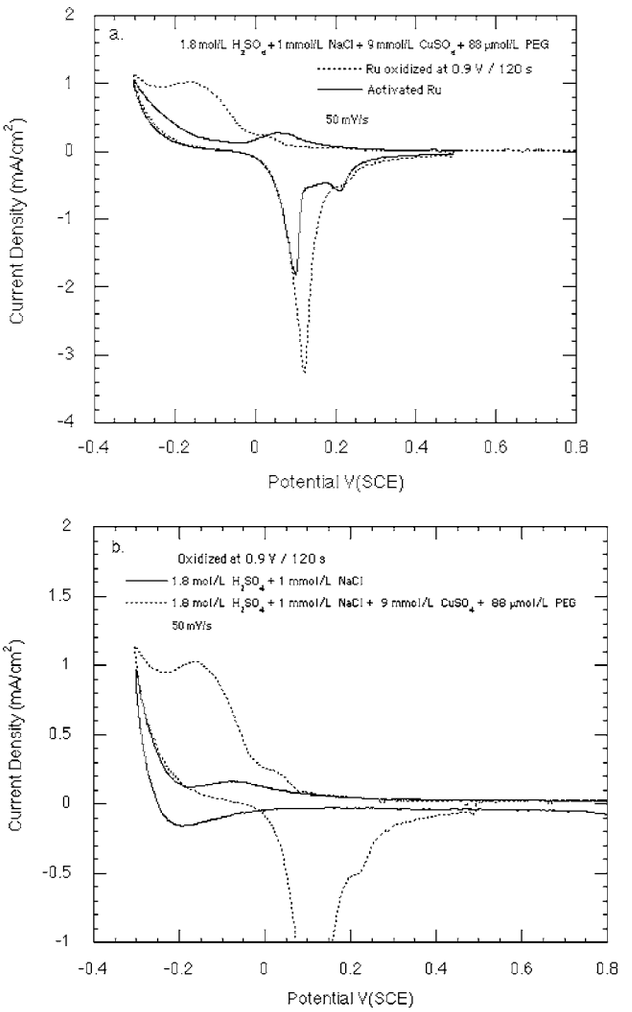

Figure 10. (a) Ru oxidation results in negligible Cu upd, while at overpotentials the nucleation and growth of Cu occurs at a rate that far exceeds that associated with overpotential deposition on the PEG/Cl/Cu upd layer (i.e., the "activated" Ru electrode). (b) Oxide reduction occurs at potentials associated with bulk Cu deposition.

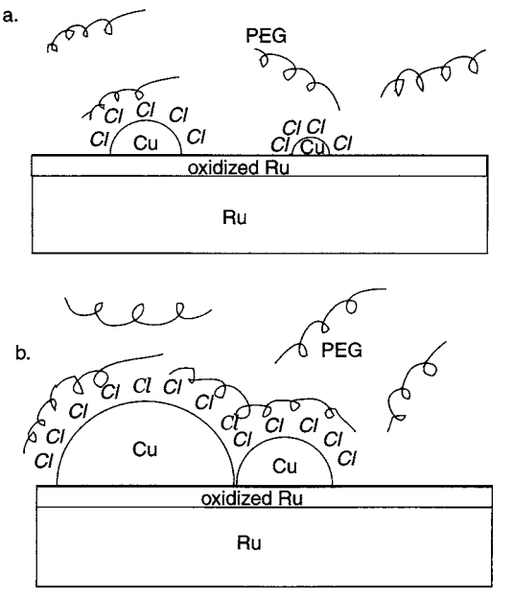

Figure 11. Bulk Cu nucleation and growth on oxidized Ru occurs by the Volmer-Weber growth mode. (a) Initially the rapid expansion of the interfacial area of the nuclei greatly exceeds the ability of PEG to accumulate and passivate the surface. (b) As the rate of area expansion decreases the PEG-Cl passivating layer begins to form, leading to the onset of inhibition.

Optical examination of an electrodeposit after 60 s reveals a rough discontinuous layer characteristic of the precoalescence stage of Volmer-Weber growth.

The same experiment was repeated at −0.2 V SCE as shown in Fig. 13b. This potential corresponds to a typical value used for superfilling submicrometer trenches. Voltammetrically (Fig. 12) the Cu and Ru electrodes are indistinguishable at this potential because the Ru surface is completely covered by Cu. In contrast, clear differences are evident during the first 70 s of the respective current transients, corresponding to the passage of approximately 0.310 C/cm^2. The initial current spike for growth on as-received Ru is much higher than for Cu, although the transients subsequently cross after 5 s. By this time a 20 mC/cm^2 film (7.3 nm equivalent of Cu) has been deposited on the Cu, while twice that amount, 47 mC/cm^2 ($\approx$17 nm equivalent of Cu), has been deposited on Ru. The PEG-Cl film forms rapidly on Cu during immersion through the air-water interface. In contrast, ellipsometry experiments indicates that a full PEG-Cl layer does not form on oxidized Ru.[24] Thus, the inhibiting PEG layer only begins to form after Cu nuclei appear (or alternatively, after oxide reduction has occurred). In the case of Cu nuclei growing on oxidized Ru, the surface coverage of PEG evolves as a competition between its accumulation from the electrolyte versus the dilution effect associated with the rapidly expanding surface area of the growing Cu nuclei, as indicated schematically in Fig. 11. The −0.2 V transients for growth on oxidized Ru and Cu merge earlier than the corresponding −0.025 V transients, suggesting a higher nuclei density, faster growth, and consequently earlier coalescence. According to Fig. 3, Fig. 5, and Fig. 10b, oxide reduction can occur in parallel with bulk Cu deposition. Thus, details of oxide formation on Ru and the extent of its subsequent reduction are expected to exert a large effect on the rate of formation and distribution of Cu nuclei.

Similar voltammetric and chronoamperometric behavior is observed for Cu deposition on glassy carbon as shown in Fig. 14. Because coinage metal deposition on glassy carbon[33] is known to proceed by the growth and coalesence of 3D nuclei, the similarity of

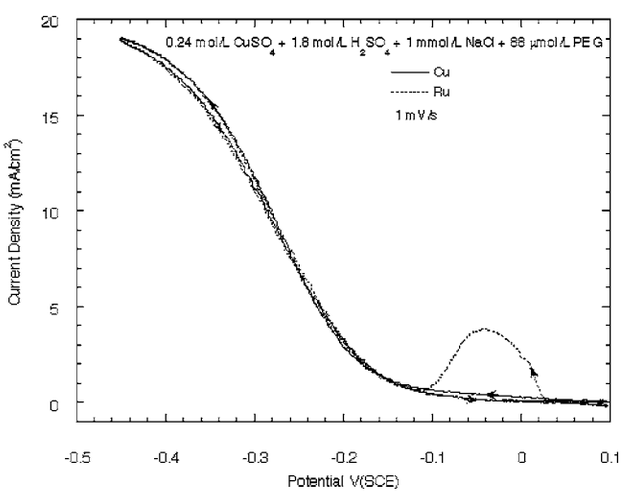

Figure 12. Slow scan voltammetry of Cu deposition on Cu and as-received Ru. The deposition wave at small overpotentials corresponds to Volmer-Weber growth on the oxidized Ru surface.

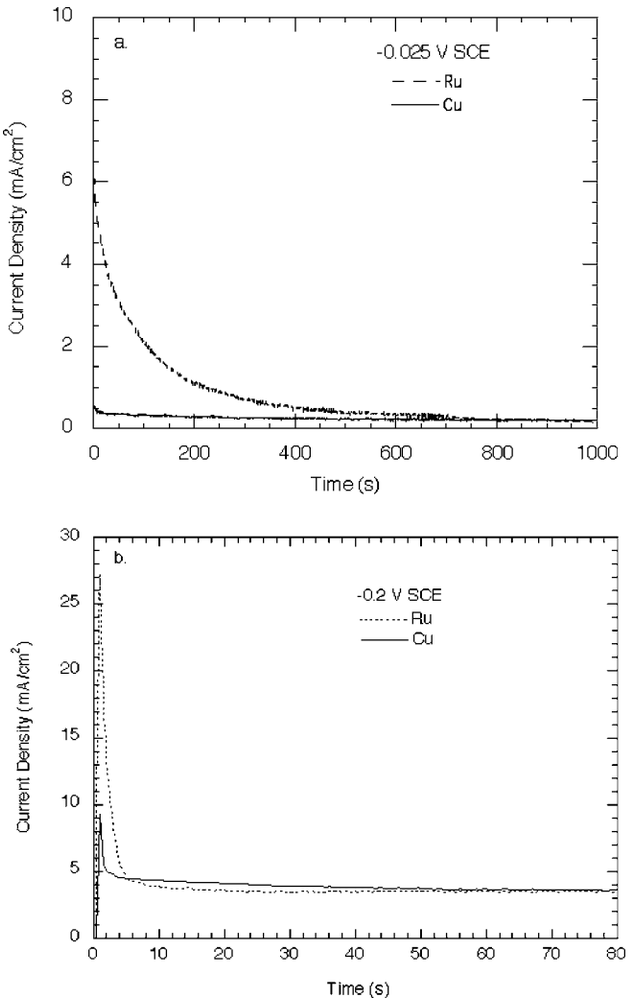

Figure 13. Chronoamperometry of Cu deposition on Cu and as-received Ru. (a) −0.025 V and (b) −0.2 V. A significant delay in the onset of PEG-Cl inhibition is evident during Volmer-Weber Cu growth on oxidized Ru.

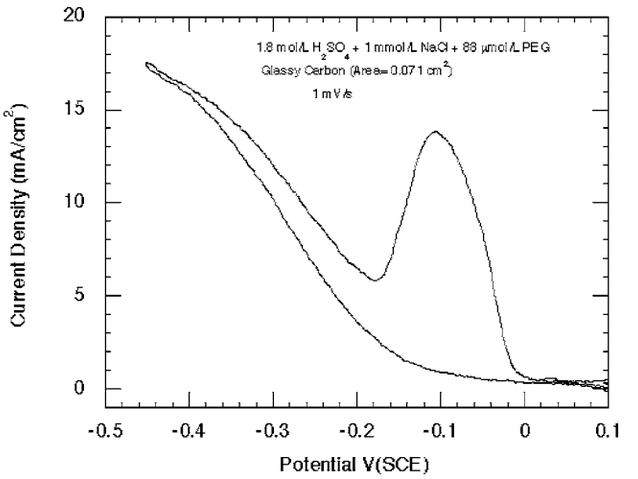

Figure 14. Slow scan voltammetry of Cu deposition on glassy carbon. The similarity to Cu deposition on oxidized Ru (Fig. 12) suggests that the peak at low overpotential is a general result of Volmer-Weber growth in the presence of slowly accumulating inhibitor.

electroanalytical measurements for Cu deposition on oxidized Ru and glassy carbon suggests this is a more general response of Volmer-Weber growth in the presence of an accumulating inhibitor that absorbs on the deposited material. The differences in shape, position, and magnitude of the ≈ -0.1 V peak (Fig. 14 vs Fig. 12) reflect difference in the details of the nucleation process and the distribution and interplay between growing nuclei. Looking to the future, the quenching of the Cu deposition rate on freshly formed nuclei may provide a useful vehicle for detailed investigations into the dynamics and formation of the PEG-Cl blocking layer. In particular, excellent temporal resolution of the initial electrode conditions can be attained, a situation that is difficult to establish using bulk Cu electrodes. Likewise, related microelectrode studies might facilitate a more detailed assessment of the growth of single nuclei.

For completeness, note that the shape of the wave at small overpotentials is congruent with prior measurements of Cu^+ activity during Cu^{2+}/Cu reduction,[34-36] although the magnitude of the latter is substantially smaller. It is possible that, in the absence of nucleation by coalesence of individual reduced metal adatoms, Cu clusters might form by a disproportionation reaction ($2Cu^+ \rightarrow Cu^{2+} + Cu$). Similarly, the possibility of CuCl precipitation should also be considered.[37,38] In any case, the sharp onset of current is suggestive of a classical heterogeneous nucleation triggered process.

In contrast to the Volmer-Weber-type growth that characterizes Cu deposition on oxidized Ru, deposition on activated Ru results in voltammetric behavior that is, comparatively speaking, indistinguishable from Cu deposition on Cu as seen in Fig. 15. The voltammetric wave at small overpotentials, associated with Volmer-Weber growth of Cu on oxidized Ru, is absent during deposition on activated Ru electrodes, although the wave can be regenerated by intentionally oxidizing a previously activated Ru electrode prior to plating, as shown in Fig. 15. From a process design perspective, the selection of a given Ru preteatment, oxidation versus reduction, dictates the growth mode during Cu deposition. In the case of Ru electrodes exposed to minor oxidation, a mixture or spatial distribution of the two Cu growth modes is possible when oxide reduction occurs on a time scale similar to that for metal nucleation. According to the literature, more severe oxidation than that employed in this work (>1.3 V SCE) may result in oxides that are not reduced by the standard activation treatment[17,18] used herein, although an intriguing report suggests that such films may support Cu upd.[29]

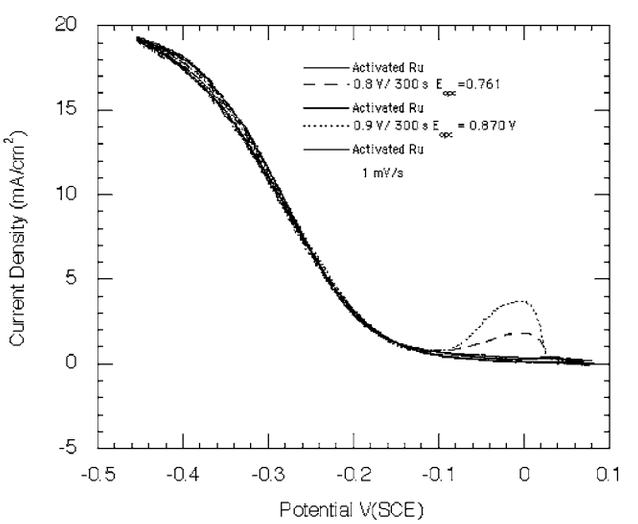

Figure 15. The voltammetric wave at small overpotentials is not observed on an activated Ru electrode. However, the wave is observed if the activated electrode is oxidized at positive potentials prior to Cu deposition.

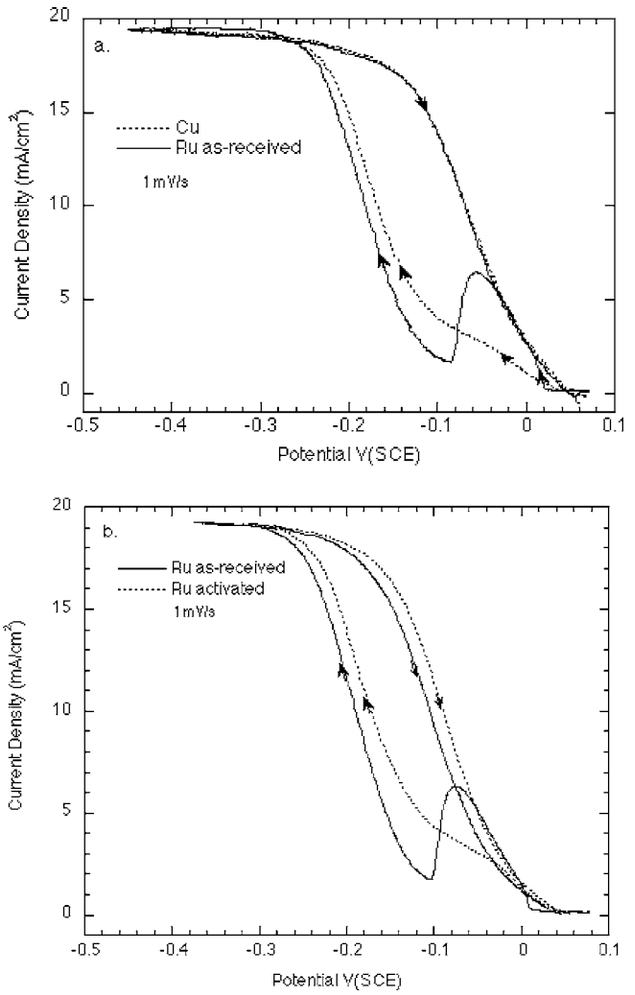

Figure 16. (a) Slow scan voltammetry of Cu deposition from a superfilling PEG-Cl-SPS electrolyte on a Cu versus an as-received Ru electrode. In addition to the hysteresis associated with the competitive interaction between PEG and SPS, the wave associated with Volmer-Weber Cu deposition on oxidized Ru is evident at small overpotentials. (b) The result for activated Ru is similar to that for a Cu electrode.

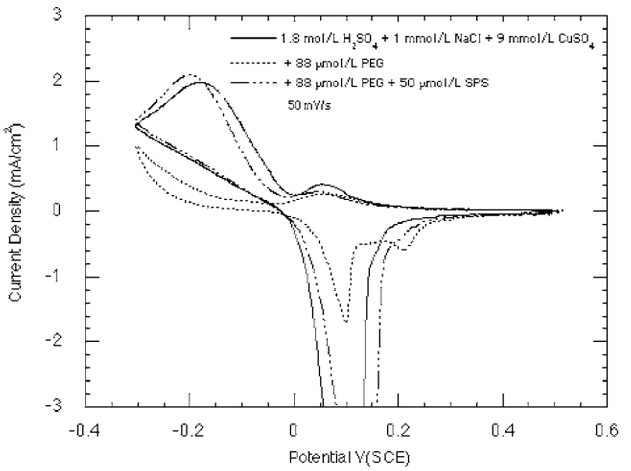

Figure 17. In a more dilute $CuSO_4$ electrolyte SPS competes very effectively with PEG coadsorption during Cu upd on an activated Ru electrode. As a consequence the PEG derived inhibition of bulk Cu deposition is significantly weakened.

SPS additions.— Superfilling submicrometer features requires the addition of a rate-accelerating additive to the PEG-Cl electrolyte, a prototypical example being SPS.[31,32] The addition of 50 μmol/L SPS to the PEG-Cl plating electrolyte results in hysteretic voltammetric behavior as shown in Fig. 16. The hysteresis is associated with the progressive potential-dependent displacement of the inhibiting PEG-Cl blocking layer by adsorption of SPS, as has been described elsewhere.[31,32] A Ru electrode activated in H_2-saturated H_2SO_4 and rapidly transferred wet for voltammetric analysis in the plating electrolyte yields a result that is essentially indistinguishable from that for a Cu electrode. In contrast, Cu deposition on air oxidized Ru is characterized by a sharp onset of uninhibited Cu deposition at 0.02 V SCE that is subsequently quenched by PEG adsorption forming a peak centered at −0.06 V. Microscopic examination of the Ru electrode after polarization at −0.05 V SCE for 30 s reveals the presence of numerous Cu clusters associated with the Volmer-Weber growth mode. The initial stage of Cu deposition on oxidized Ru is analogous to that observed in the absence of SPS. In contrast, for a given growth potential or program, substantially smoother films are observed during deposition on activated Ru.

Chronoamperometry studies of Cu deposition from a SPS-Cl-PEG electrolyte are typically associated with rising current transients that reflect the displacement of the PEG-Cl blocking layer by SPS adsorption.[31,32] As would be expected, this overall trend is also evident for Cu deposition on oxidized Ru once coalescence has occurred. In contrast, significant deviation is apparent during the first 20 s of Cu deposition at −0.2 V SCE, a typical potential used in superfilling experiments. An additional charge of ≈50 mC/cm^2 (approximately 20% more Cu) is deposited on the as-received, oxidized Ru, as compared to growth on a planar Cu electrode, due to the nonplanar growth morphology. The global (average) deposition of 100 monolayers of Cu provides an upper bound estimate for the thickness required to obtain a coalesced copper overlayer at this potential. Use of activated Ru allows the upper bound to be significantly reduced.

In order to investigate the competitive interaction between SPS and PEG and the Cl-upd Cu layer that forms on activated Ru, metal deposition from a dilute $CuSO_4$ electrolyte was briefly examined. As shown in Fig. 17, Cu upd on an activated Ru electrode is accompanied by SPS adsorption that significantly hinders the formation of the PEG blocking layer that otherwise forms in its absence. Thus, starting with an electrode derivatized with one particular constituent and then monitoring its evolution during metal deposition in the presence of other additives permits detailed surface analytical studies of the structure, composition, and dynamics of these important multicomponent adlayers. Indeed, the strategy of catalyst pretreatment for superfilling applications has already been successfully demonstrated on Cu substrates.[31,32,39]

SPS derivatization.— Catalyst pretreatment of Ru provides an opportunity to exploit the above scheme free of the problematic complications associated with corrosion of conventional Cu-seeded substrates. As in the case of Cu upd, the reactivity of Ru towards molecular adsorption is a strong function of its initial surface state.[40] XPS examination of the Ru electrodes derivatized in a 500 μmol/L SPS + 1.8 mol/L H_2SO_4 electrolyte reveals that significant disulfide or thiol adsorption only occurs at negative potentials where the air-formed, passivating surface layer is removed. As shown in Fig 18, Ru immersion in an aerated electrolyte at the open-circuit potential (0.69 V SCE) for 300 s leads to negligible disulfide or thiol formation. In contrast, immersion with the potential held at 0.0 or −0.2 V SCE for 300 s leads to formation of a thiol/disulfide-sulfonate film, as evidenced by the thiolate or disulfide peak at 162.7 eV and the sulfonate peak at 167.7 eV. The intensity of the disulfide/thiol signal increases with negative potential, suggesting the possibility that the Ru substrate is sulfided under these circumstances. In a related fash-

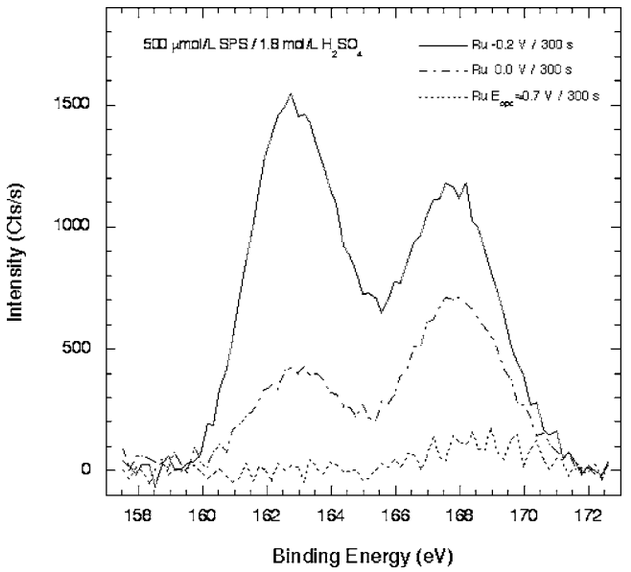

Figure 18. XPS examination of disulfide adsorption on Ru. A monolayer disulfide/thiol film is formed rapidly at negative potentials, i.e., coincident with oxide reduction. The increase in the ratio of disulfide/thiol (162.7 eV) to sulfonate (167.7 eV) suggests that Ru is sulfided at more negative potentials.

ion, irreversible changes are evident during multicycle voltammetric probing of SPS coadsorption with Cu upd on activated Ru. Namely, a monotonic decrease in the Cu upd peak occurs with time in the presence of SPS-PEG-Cl (Fig. 19) that is not evident in the presence of PEG-Cl. A recent UHV report[13] describes coverage-dependent sulfide formation resulting from the interaction between adsorbed H_2S and a strained Cu monolayer on Ru(0001). Further analytical work will be required to sort out the various interactions occurring between Cu upd, halide and thiol/disulfide adsorption, and the consequence of sulfide formation. Nevertheless, the activity of an SPS-derivatized Ru electrode towards bulk Cu deposition in an SPS-free PEG-Cl electrolyte was briefly examined. The as-received Ru electrodes were derivatized under potential control in the respective 500 µmol/L SPS/1 mmol/L MPS sulfuric acid electrolyte, rinsed in 1.8 mol/L H_2SO_4, and then immersed under potential control

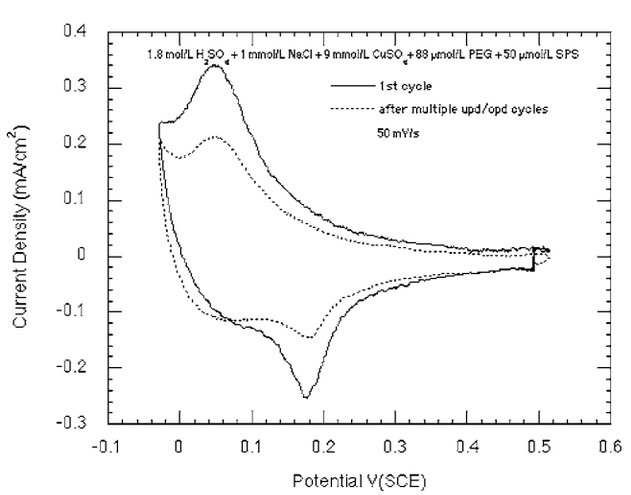

Figure 19. The addition of SPS to the PEG-Cl electrolyte results in Cu upd on Ru evolving substantially with time. The most notable change is a decrease in the deposition and stripping charge with potential cycling.

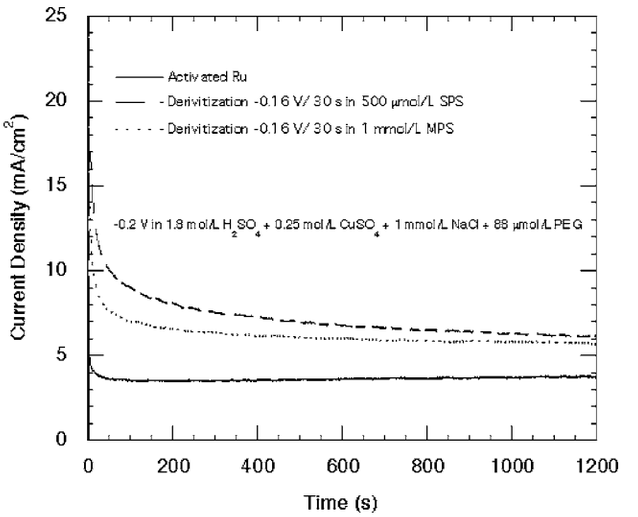

Figure 20. Chronoamperometry behavior for activated Ru electrodes showing the catalytic effect of SPS derivatization and its persistence during Cu plating.

−0.2 V SCE in the PEG-Cl Cu plating bath. As in the case of Cu electrodes,[31,32] SPS derivatization of activated Ru results in significant acceleration of the Cu deposition rate, as revealed by the sharply increased current at early times in Fig. 20. However, unlike derivatized Cu electrodes[31,32] where deactivation occurs over a period of thousands seconds, substantial deactivation of the derivatized Ru electrodes occurs in the first 100 s. Nevertheless, some catalytic activity is sustained even after ≈3 µm of Cu deposition. More work examining the details of formation and structure of SPS on Ru versus the SPS on Cu will be required to sort out the different dynamics, particularly deactivation, associated with the respective electrodes.

Influence of Ru pretreament on Cu damascene processing.— The previous electroanalytical studies and optical inspection reveal that the surface state of Ru has a dramatic effect on the morphology of Cu electrodeposits. As-received Ru is covered with an air-formed oxide film, the thickness of which depends on the humidity, temperature, and exposure time.[22,23] If oxidation exceeds a monolayer the film may only be reduced at potentials below that required to deposit Cu (e.g., Fig. 10b). Consequently, Cu upd is not observed on the 3D oxide formed on Ru. Bulk Cu deposition still occurs on the nonwetting oxide surfaces; however, the growth proceeds following the Volmer-Weber model, resulting in rough Cu films at the point of coalescence. Activation of as-received Ru by polarization into or near the hydrogen evolution region results in a metallic surface that readily forms a upd Cu monolayer film. As will be shown, the wetting layer facilitates the deposition of comparatively smooth compact bulk Cu films. The upd process is readily observed provided oxidation of the activated surface is restricted to the formation of a monolayer oxide. Under such conditions the kinetics of formation of the upd layer appears to be limited by the rate of reduction of the monolayer oxide. The important consequences of the initial state of the Ru layer on Cu adhesion and seedless superfilling were examined.

Adhesion.— Ru pretreatment exerts a marked effect on the adhesion of electroplated Cu. This was examined by attempting to peel a ≈1 µm thick plated Cu film away from the Ru/Ti/SiO_x/Si(100) substrate. A cleavage crack was first inserted into the Si substrate, leaving the two halves still connected by the overlying metal film. One half of the substrate was then pulled orthogonally away from the other. Optical inspection, i.e., the color of the back-side of the peeled metal film, provided a clear indication of the location of

adhesion failure. Cu films deposited on the as-received, air oxidized $Ru/Ti/SiO_x/Si(100)$ substrates peeled cleanly at the Cu/Ru interface due to the presence of the oxide. In contrast, when the Ru substrate was activated prior to Cu deposition, failure occurred at the $Ru/Ti/SiO_x/Si$ interface. Thus, a more robust metallic bond is formed between the electrodeposited Cu and the reduced Ru surface.

Morphological evolution and the "terminal effect.".— When depositing on thin resistive seed layers, severe potential variations, known as the "terminal effect," may occur as a function of distance from the electrode contact.[41] For potentiostatic deposition in an additive-free electrolyte, where the growth rate is a monotonic function of overpotential, the iR potential drop increases with distance from the contact. In severe cases this results in significant lateral motion of the propagating growth front away from the contact as the deposited film becomes more conductive. Creative approaches to electrochemical cell design and process control have been explored to ameliorate this problem.[41-44] The effect of counter electrode position, Tafel kinetics, and mass transfer limitations for metal deposition have been explored.[41] Nucleation on a foreign substrate combined with serial or parallel oxide reduction, as it applies to these Cu on Ru studies, remains to be fully considered. However, according to nucleation theory, the size, density, and distribution of nuclei are strong functions of overpotential with the density typically increasing with overpotential. The terminal effect enables these relationships to be rapidly evaluated by examining the deposit as a function of distance from the electrode contact, a combinatorial vehicle of sorts. Consideration of local electrical gradients may be necessary as they can be highly nonuniform, at least until nuclei coalescence occurs on top of the resistive seed layer. Deposition in the presence of an inhibitor, such as PEG-Cl, provides a further complication, particularly when growth proceeds along the Volmer-Weber pathway. As observed in Fig. 12, the rapid initial growth of uninhibited nuclei followed by passivation results in an inversion or nonmonotonic
η-i response. The convolution of these effects can result in significant microstructural heterogeneity as a function of distance from an electrode contact. For example, Fig. 21 shows that deposition for 10 s at −0.2 V in the PEG-Cl electrolyte leads to high nucleation density and film coalescence near the contact, with the nuclei size increasing and the density decreasing moving away from the contact. A bimodal distribution of nuclei, resulting from the potential transiting the inverted region of the η-i curve, is evident at 9 mm from the contact. At points further removed from the consolidated growth front, individual nuclei may still grow quite rapidly at the start of deposition, as the small number of nuclei makes the overall current density, and associated iR drop, small in spite of the high local current density on discrete nuclei. More complete knowledge of the nucleation probability and distribution function as a function of potential should enable simulations of the convolution of the terminal effect with Volmer-Weber growth in the presence of an inhibitor. Nonetheless, it is clear that such deposition is completely unacceptable in the context of damascene processing where the individual nuclei shown greatly exceed the dimensions of technically relevant features. Attention is therefore focused on strategies to circumvent this problem. Chief among these is minimization of Ru oxidation prior to Cu deposition. This may be implemented by either (*a*) maintaining an inert atmosphere between Ru deposition and Cu plating; (*b*) performing a Ru oxide removal or activation treatment prior to Cu deposition; or (*c*) using capping treatments after Ru deposition. The latter might involve capping with an ultrathin vacuum deposited Cu layer or perhaps some other protective or even activating adsorbate, e.g., iodine[45-47] or palladium.[48,49]

As shown previously, the inverted η-i behavior is not observed on an activated Ru electrode (i.e., Fig. 15). Morphological evolution during Cu deposition on an activated versus an aged as-received 6.5 nm thick Ru seed layer is quite distinct. The difference between the two substrates during growth from a superfilling electrolyte is obvious to the eye. The Cu film grown on activated Ru is specular in nature, while the film deposited on oxidized Ru is rough. FE-SEM images of the respective surfaces are shown in Fig. 22 as a function of distance from the electrode contact. Deposition on the aged as-received Ru seed is analogous to that observed in Fig. 21 in the PEG-Cl, namely a rough coalesced film near the contact, transitioning with distance to a bimodal distribution of nuclei, and finally large individual nuclei at points further away. In contrast, deposition on the activated electrode revealed a fully coalesced film that was substantially smoother. A slight increase of roughness with distance from the contact possibly reflects decreasing nucleation density at lower overpotential due to iR drop.

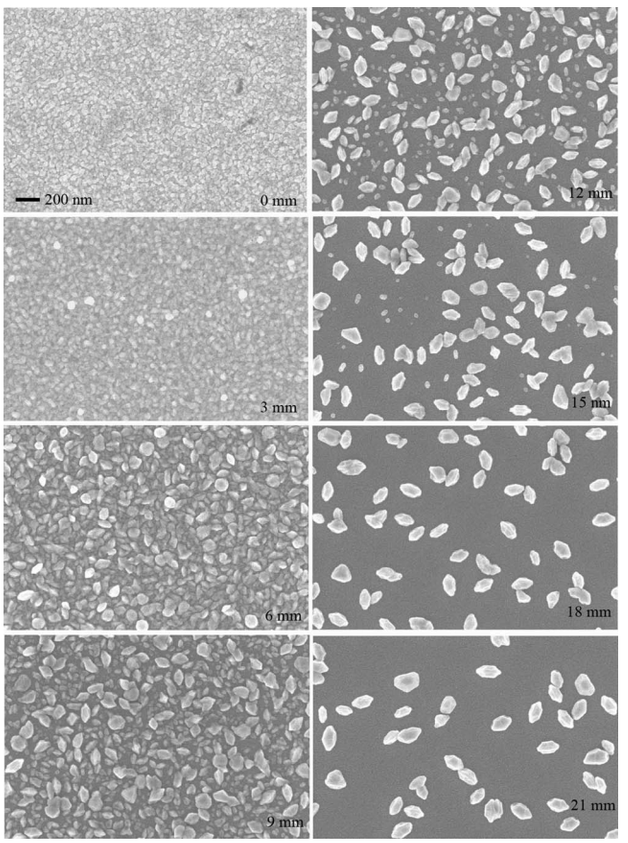

Figure 21. FE-SEM images demonstrating the convolution of the "terminal effect" and potential-dependent microstructural evolution during Cu deposition on an aged Ru seed layer. The images are shown as a function of distance (3 mm increments) from the electrode contact. Cu was deposited at −0.2 V for 10 s in the PEG-Cl electrolyte. The Ru seed layer was 27 nm thick.

Feature filling studies.— Feature superfilling by direct Cu deposition on Ru seed layers was examined as a function of surface treatment and plating conditions. Effective trench filling was accomplished by rapid immersion (i.e., plunging) a freshly PVD deposited Ru seed wafer fragment into a PEG-Cl-SPS electrolyte with the potential applied at −0.2 V SCE. As shown in Fig. 23, complete coalescence of the Cu layer is obtained by 3.4 s of deposition. Subsequent growth follows the bottom-up filling dynamic associated with preferential enrichment of the accelerating SPS-derived catalyst on the concave surface, as described by the CEAC mechanism.[32] For this particular chemistry the sloping sidewalls contribute substantially to void-free bottom-up filling for feature aspect ratios greater than 2. In this instance the process is able to fill trenches with midheight width of $\approx$50 nm.

Superfill through pulse plating was also examined using a three-pulse scheme. The as-received specimen was first placed in the elec-

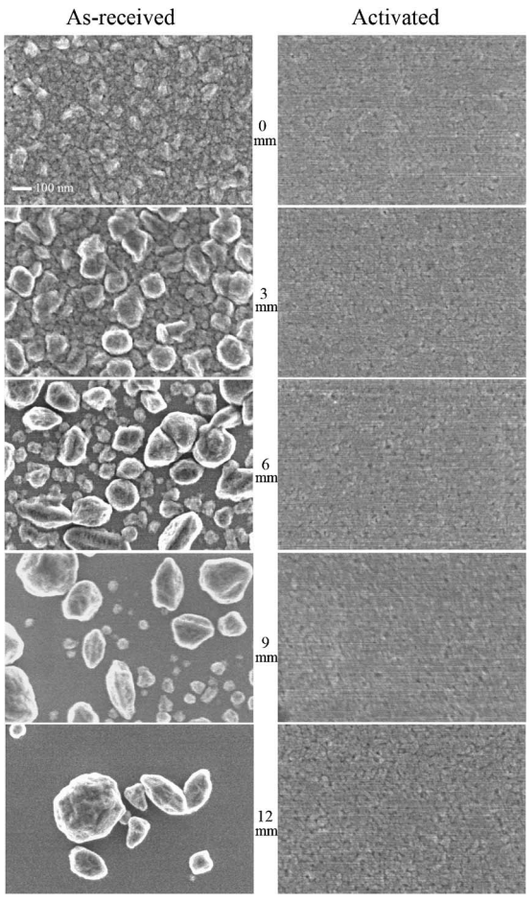

Figure 22. FE-SEM images demonstrating the influence of the Ru surface conditions and the "terminal effect" on morphological and microstructural evolution during Cu deposition. Cu was deposited at −0.2 V for 30 s in a PEG-Cl-SPS electrolyte. The Ru seed layer was 7 nm thick.

trolyte with the potential set at +0.1 V SCE. After 30 s the potential was stepped to −0.4 V SCE for 1 s followed by −0.2 V SCE for the duration of the experiment. As shown in Fig. 24, the shape of the resulting growth contours is indistinguishable from that observed for potentiostatic deposition on a freshly evaporated Ru film (i.e., Fig. 23). As noted earlier, depending on the extent of Ru oxidation, the first step likely involves reduction of the monolayer oxide, followed by Cu upd as well as coincident additive adsorption. The second step would lead to rapid reduction of any residual 3D oxide in combination with nucleation and coalescence of the Cu layer. The final potential corresponds to the value used to superfill submicrometer features in one step. The relative contributions of the respective processes to successful feature filling remain to be fully determined, but indications are that the most important aspect to successful feature filling is the nature of the oxide on the as-received surface.

The sensitivity to initial conditions was directly investigated by comparing Cu deposition morphology on two Ru samples that had received simultaneous (thus identical) processing prior to wet processing. One sample was immediately plunged into the PEG-Cl-SPS electrolyte with potential −0.2 V SCE applied. The other specimen was first oxidized at +0.9 V SCE for 300 s, then released to open-circuit conditions for a few seconds in the stagnant electrolyte (open to the atmosphere), and then plated at −0.2 V SCE for roughly the same period of time as the first specimen. As shown in Fig. 25, the well-defined bottom-up superfilling behavior that is evident on a freshly evaporated Ru surface is destroyed by intentional oxidation, resulting in poor wetting and void formation within the trench.

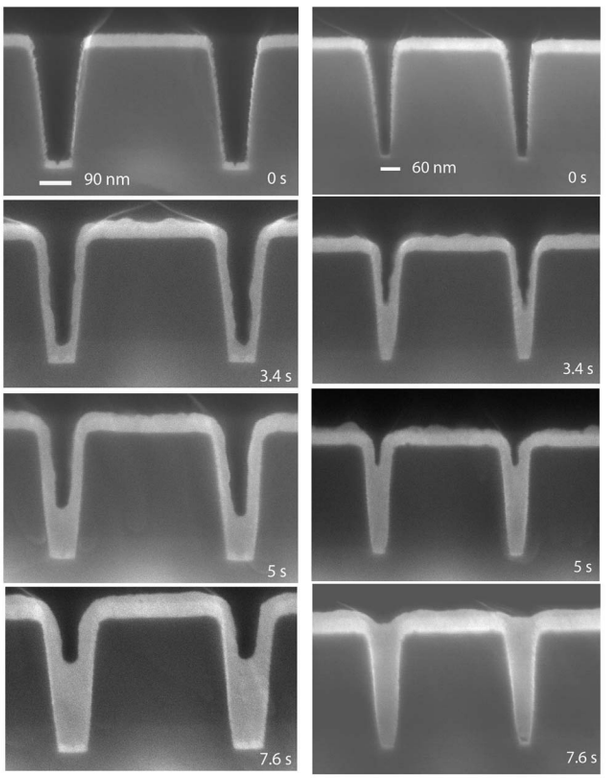

Figure 23. FE-SEM cross-section images of Cu superfilling of trenches [≈90 nm (left) and ≈50 nm (right) in width at midheight] covered with a freshly deposited PVD Ru barrier layer. Patterned substrates were immersed at −0.2 V in the PEG-Cl-SPS for the specified period of time.

A further demonstration of the importance of controlling Ru oxidation is demonstrated by comparing Cu deposition on two identical Ru-seeded wafer fragments that were left in the laboratory ambient for 1 week. Direct deposition on the aged as-received specimen resulted in the formation of a relatively low density of discrete Cu

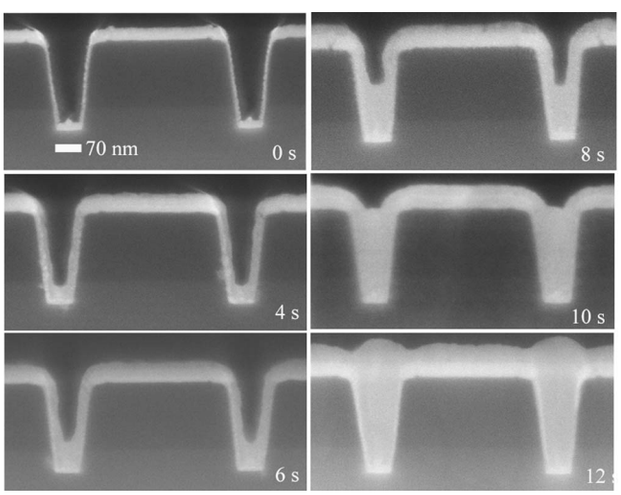

Figure 24. FE-SEM cross-section images of Cu superfilling using pulse plating in the PEG-Cl-SPS electrolyte. The patterned PVD Ru electrode was immersed at +0.1 V for 30 s. Deposition was initiated by pulsing the potential to −0.4 V for 1 s and then stepping to −0.2 V for the duration of the experiment.

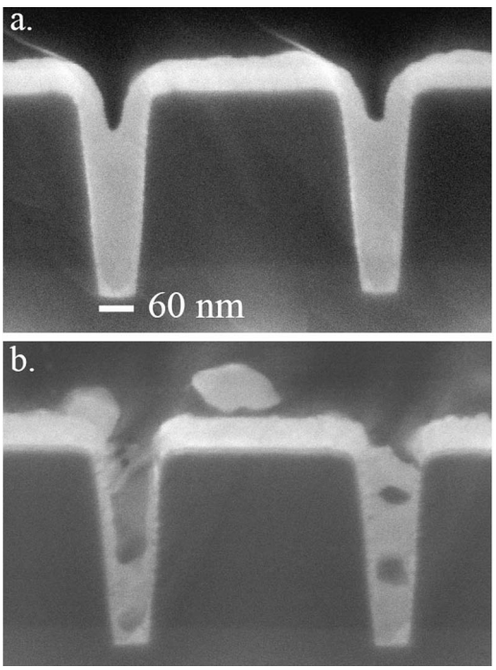

Figure 25. The detrimental effect of Ru oxidation on trench filling is shown. Cu was deposited at −0.2 V for 7.6 s on (a) freshly deposited Ru barrier. (b) Ru electrochemically oxidized at 0.9 V for 300 s.

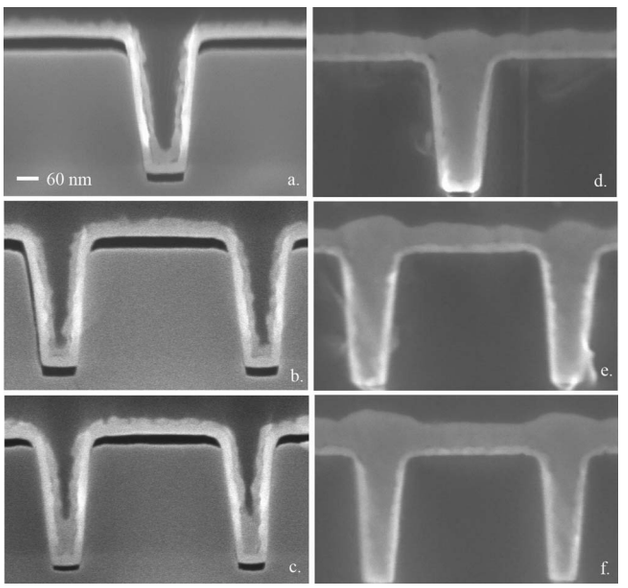

Figure 27. Cu superfilling of trenches lined with a Ru ALD barrier layer. Pulse plating was utilized; the specimens were first immersed at +0.1 V for 30 s, followed by pulsing to −0.4 V for 1 s and then stepping to −0.2 V for (a, b, c), 6 s and (d, e, f), 18 s, respectively. The extended filling time associated with deposition on the ALD barrier may be attributed to the terminal effect.

nuclei as shown in Fig. 26a and b. In contrast, when the aged specimen was activated by immersion in H_2-saturated 1.8 mol/L H_2SO_4 (>20 min) and then transferred for plating, complete coalescence of the Cu layer was obtained before bottom-up filling of the trench began (Fig. 26c and d). Unlike previous images, these specimens were grown at a low overpotential, corresponding specifically to the peak of the inverted region of the η-i curve for oxidized Ru (−0.05 V in Fig. 16). Optical observations of deposits grown on activated electrodes at such low overpotentials are much rougher than those grown at the higher potentials typically used in damascene processing (compare Fig. 23 and Fig. 26). Thus, these experiments represent the most challenging conditions that might be anticipated during feature filling on extremely resistive seed layer. This test further exaggerated this difference by growing for an extended period of time (30 s); in practice, Cu deposition on a resistive seed layer would experience growth at such low potentials for only a short period of time before coalescence would eliminate the local iR drop and the growth rate would accelerate into the regime where effective CEAC smoothing occurs.

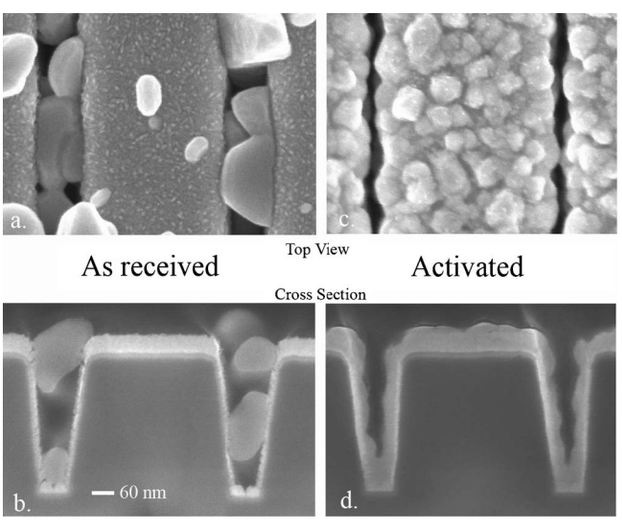

Figure 26. Electrodeposition on an aged as-received Ru film leads to poor wetting and gross failure in feature-filling experiments. In contrast, activation of the same Ru film prior to Cu electrodeposition results in coalescence of the Cu layer in time for effective feature filling to occur. Cu was deposited at −0.05 V for 30 s in PEG-Cl-SPS. Note that growth at small overpotentials on activated Ru results in rougher films than observed at greater overpotentials.

Close examination of the sidewalls of the PVD Ru layer (e.g., 0 s in Fig. 23 and 24) reveals significant porosity and roughness that will compromise the performance of the final structure. Because the thin, rough sidewall coverage is a direct consequence of the oblique PVD deposition in those locations, an ALD barrier deposition process capable of generating smooth conformal layers was examined. The three-pulse deposition scheme effectively filled the ALD-seeded trenches as shown in Fig. 27, consistent with the results on the PVD Ru films in Fig. 24. Delamination at the $Ru/Al_2O_3/SiO_x$ dielectric interface occurred subsequent to deposition, during cross sectioning; it affects the quality of the images by degrading the planarity of the cross sections without affecting interpretation of the filling.

In other potentiostatic experiments (not shown here), deposition on the as-received surface (after transatlantic shipping) resulted in poor wetting and Volmer-Weber growth due to the surface oxide. A more favorable surface state was generated on these samples by immersion in a H_2-saturated 1.8 mol/L H_2SO_4 electrolyte (>20 min) prior to electrodeposition. Complete gap filling was then obtained, although the resistive nature of the very thin ALD Ru barrier resulted in longer filling times than observed for the thicker PVD barrier layers.

Conclusions

Seedless superfilling of submicrometer trenches by direct Cu electrodeposition onto PVD and ALD Ru barriers was investigated. The nucleation and growth mode of electroplated Cu is a function of the state of oxidation of the Ru surface as well as the Cu deposition

parameters. Whether Cu deposition occurs competitively with oxide reduction depends on the processing conditions. The 3D oxide formed on Ru exposed to the laboratory ambient can be reduced by polarization in the hydrogen evolution region. Subsequent oxidation is limited to the monolayer regime provided the potential is held below +0.5 V SCE. Reduction of the oxide monolayer occurs at potentials coincident with Cu upd and can control the deposition kinetics of the latter. PEG interacts with halide and the Cu upd layer to form a passivating layer that inhibits bulk Cu deposition in a manner analogous to that formed on a bulk Cu electrode. The upd layer also interacts irreversibly with SPS, a standard catalyst used in superfilling electrolytes. The Cu upd layer may act as a wetting layer for subsequent Cu overpotential deposition. The interaction between Cu upd and the plating additives and their combined influence on bulk Cu deposition offers interesting technological possibilities as well as a model system for more detailed scientific study. Activated Ru layers, or Ru layers that are otherwise free of thick oxide, are shown to be suitable for seedless Cu superfilling of sub-100 nm features. Pulse plating is also seen to be potentially useful for ensuring complete oxide reduction and high nucleation density of bulk Cu. Deposition on a reduced oxide-free Ru surface results in more rapid coalescence involving the formation of a wetting Cu upd layer as well as improved adhesion between Cu and Ru.

In contrast to activation, extended exposure of Ru to the laboratory environment or electrochemical oxidation above >0.5 V SCE results in the formation of a 3D oxide. This oxide blocks Cu upd as well as additive adsorption, while bulk Cu deposition follows the Volmer-Weber growth mode. Initially, the rapid area expansion of the nuclei growth front overwhelms the ability of PEG-Cl to inhibit growth, resulting in very rough deposits. Oxide reduction can occur competitively with bulk Cu deposition and can influence the nucleation process. However, the remaining oxide results in weak adhesion between Cu and Ru, and a low nucleation density that leads to poor trench filling. These effects are accentuated on thin resistive oxide-covered Ru seed layers due to coupling of the terminal effect with the inverted η-i response that allows for rough Volmer-Weber growth at lower potentials.

National Institute of Standards and Technology assisted in meeting the publication costs of this article.

References

1. A. Radisic, Y. Cao, P. Taephaisitphongse, A. C. West, and P. C. Searson, *J. Electrochem. Soc.*, **150**, C362 (2003).
2. A. Radisic, G. Oskam, and P. C. Searson, *J. Electrochem. Soc.*, **151**, C369 (2004).
3. O. Chyan, T. N. Aunagiri, and T. Ponnuswamy, *J. Electrochem. Soc.*, **150**, C347 (2003).
4. D. Josell, D. Wheeler, and T. P. Moffat, *Electrochem. Solid-State Lett.*, **6**, C143 (2003).
5. M. W. Lane, C. E. Murray, F. R. McFeely, P. M. Vereecken, and R. Rosenberg, *Appl. Phys. Lett.*, **83**, 2330 (2003).
6. Z. Sun, R. He, and J. O. Dukovic, *Proceedings of the Advanced Metallization Conference 2004*, D. Erb, P. Ramm, K. Masu, and A. Osaki, Editors, p. 531, The Materials Research Society, Pittsburgh (2005).
7. C. Nguyen Van Huong and M. J. Gonzalez-Tejera, *J. Electroanal. Chem. Interfacial Electrochem.*, **244**, 249 (1988).
8. M. A. Quiroz, Y. Meas, E. Lamy-Pitara, and J. Barbier, *J. Electroanal. Chem. Interfacial Electrochem.*, **157**, 165 (1983).
9. K. R. Zavadil, D. Ingersoll, and J. W. Rogers, *J. Electroanal. Chem. Interfacial Electrochem.*, **318**, 223 (1991).
10. E. M. Stuve, J. W. Rogers, D. Ingersoll, D. W. Goodman, M. L. Thomas, and M. T. Paffett, *Chem. Phys. Lett.*, **149**, 557 (1988).
11. G. O. Potschke and R. J. Behm, *Phys. Rev. B*, **44**, 1442 (1991).
12. C. Gunther, J. Vrijmoeth, R. Q. Hwang, and R. J. Behm, *Phys. Rev. Lett.*, **74**, 754 (1995).
13. J. Hrbek, J. De la Figuera, K. Pohl, T. Jirsak, J. A. Rodriguez, A. K. Schmid, N. C. Bartelt, and R. Q. Hwang, *J. Phys. Chem. B*, **103**, 10557 (1999).
14. J. X. Wang, N. S. Marinkovic, H. Zajonz, B. M. Ocko, and R. R. Adzic, *J. Phys. Chem. B*, **105**, 2809 (2001).
15. N. S. Marinkovic, J. X. Wang, H. Zajonz, and R. R. Adzic, *J. Electroanal. Chem.*, **500**, 388 (2001).
16. M. B. Vukmirovic, R. L. Sabatini, and R. R. Adzic, *Surf. Sci.*, **572**, 269 (2004).
17. D. Mitchell, D. A. J. Rand, and R. Woods, *J. Electroanal. Chem. Interfacial Electrochem.*, **89**, 11 (1978).
18. S. Hadzi-Jordanov, H. Angerstein-Kozlowska, M. Vukovic, and B. E. Conway, *J. Electrochem. Soc.*, **125**, 1471 (1978).
19. R. O. Lezna, N. R. Tacconi, and A. J. Arvia, *J. Electroanal. Chem. Interfacial Electrochem.*, **151**, 193 (1983).
20. K. Robbie and M. J. Brett, *J. Vac. Sci. Technol. A*, **15**, 1460 (1997).
21. F. Colom and M. J. Gonzalez-Tejera, *J. Appl. Electrochem.*, **24**, 426 (1994).
22. H. Yeung, H. Chan, S. Zou, and M. J. Weaver, *J. Phys. Chem. B*, **103**, 11141 (1999).
23. H. Luo, S. Park, H. Yeung, H. Chan, and M. J. Weaver, *J. Phys. Chem. B*, **104**, 8250 (2000).
24. M. Walker, L. Richter, and T. P. Moffat, *J. Electrochem. Soc.*, Submitted.
25. T. P. Moffat, J. E. Bonevich, W. H. Huber, A. Stanishevsky, D. R. Kelly, G. R. Stafford, and D. Josell, *J. Electrochem. Soc.*, **147**, 4524 (2000).
26. T. Aaltonen, P. Alén, M. Ritala, and M. Leskela, *Chem. Vap. Deposition*, **9**, 45 (2003).
27. G. Horanyi and E. M. Rizmayer, *J. Electroanal. Chem. Interfacial Electrochem.*, **181**, 199 (1984).
28. E. R. Kotz and S. Stucki, *J. Appl. Electrochem.*, **17**, 1190 (1987).
29. Y. Zhang, L. Huang, T. N. Arunagiri, O. Ojeda, S. Flores, O. Chyan, and R. M. Wallace, *Electrochem. Solid-State Lett.*, **7**, C107 (2004).
30. M. Walker, L. Richter, and T. P. Moffat, *J. Electrochem. Soc.*, **152**, C403 (2005).
31. T. P. Moffat, D. Wheeler, and D. Josell, *J. Electrochem. Soc.*, **151**, C262 (2004).
32. T. P. Moffat, D. Wheeler, M. D. Edelstein, and D. Josell, *IBM J. Res. Dev.*, **49**, 19 (2005).
33. A. Milchev and L. Heerman, *Electrochim. Acta*, **48**, 2903 (2003).
34. G. W. Tindall and S. Bruckenstein, *Anal. Chem.*, **40**, 1051 (1968).
35. G. W. Tindall and S. Bruckenstein, *Anal. Chem.*, **40**, 1637 (1968).
36. P. M. Vereecken, R. A. Binstead, H. Deligianni, and P. C. Andricacos, *IBM J. Res. Dev.*, **49**, 3 (2005).
37. K. Doblhofer, S. Wasle, D. M. Soares, W. G. Weil, G. Weinberg, and G. Ertl, *Z. Phys. Chem.*, **217**, 479 (2003).
38. W.-P. Dow and H.-S. Huang, *J. Electrochem. Soc.*, **152**, C67 (2005).
39. T. P. Moffat, D. Wheeler, C. Witt, and D. Josell, *Electrochem. Solid-State Lett.*, **5**, C110 (2002).
40. L.-Y. O. Yang, S.-L. Yau, and K. Itaya, *Langmuir*, **20**, 4596 (2004).
41. M. Matlosz, P.-H. Vallotton, A. C. West, and D. Landolt, *J. Electrochem. Soc.*, **139**, 752 (1992).
42. H. Deligianni, J. O. Dukovic, E. G. Walton, R. J. Contolini, J. Reid, and E. Patton, *Electrochemical Processing in ULSI Fabrication and Semiconductor/Metal Deposition II*, PV99-9, 83 The Electrochemical Society, Inc, Pennington, NJ (1999).
43. Y. Cao, J. M. Lee, and A. C. West, *Plat. Surf. Finish.*, **90**, 40 (2003).
44. T. L. Ritzdorf, G. J. Wilson, P. R. McHugh, D. J. Woodruff, K. M. Hanson, and D. Fulton, *IBM J. Res. Dev.*, **49**, 65 (2005).
45. J. Liu, J. Lei, N. Magtoto, S. Rudenja, M. Garza, and J. A. Kelber, *J. Electrochem. Soc.*, **152**, G115 (2005).
46. P.-C. Lu, C.-H. Yang, S.-L. Yau, and M.-S. Zei, *Langmuir*, **18**, 754 (2002).
47. H.-B. Lee, D.-K. Kwak, and S.-W. Kang, *Electrochem. Solid-State Lett.*, **8**, C39 (2005).
48. S.-K. Kim, S. K. Cho, J. J. Kim, and Y.-S. Lee, *Electrochem. Solid-State Lett.*, **8**, C19 (2005).
49. S. K. Cho, S.-K. Kim, H. Han, J. J. Kim, and S. M. Oh, *J. Vac. Sci. Technol. B*, **22**, 2649 (2004).